J. Indian Inst. Sci., Mar–Apr 1988, **68**, 79–90

Influence of ground clearance on the forces on a three-dimensional bluff body

B. H. LAKSHMANA GOWDA
Fluid Mechanics Laboratory, Department of Applied Mechanics, Indian Institute of Technology, Madras 600 036, India

Received on March 4, 1987, Revised on October 5, 1987.

Abstract

The forces and moments on a three-dimensional bluff body with a square cross-section and length-to-width ratio of four is presented in this paper. The influence of the ground clearance between the body and the ground plane on the forces and moments is brought out at various angles of yaw. The results show that both gap and yaw considerably change the aerodynamic forces and moments but the extent of their influence on the various forces and moments is not the same. Flow visualisation results are presented which offer a tentative explanation to the observed features.

Key words: Bluff body, aerodynamic forces and moments.

1. Introduction

A road vehicle is typically a three-dimensional bluff body with finite height-to-width and length-to-width ratios. In addition, there is the presence of a road surface and the flow field can be expected to be considerably influenced by the ground clearance between the vehicle and the road. Basic studies on three-dimensional bluff bodies which have dimensions comparable to those of the road vehicles are essential and fundamental to generating aerodynamically efficient road vehicles. With this as the motivation, Nakaguchi[1] has investigated forces on three-dimensional bluff bodies with square cross-section and various length-to-width ratios varying from 0 to 4·2. But he did not utilise any ground plate to simulate the road surface and as such one can expect the results to have their own limitations. The stagnation point (or line) on the front face of the body would occur at the centre of the face when there is no ground plate. With the ground surface, the location of the front face stagnation point (or line) would vary depending on the extent of ground clearance[2]. Also the flow is inhibited and restricted to flow in the gap between the body and the ground surface. This can give rise to completely different force field on the body than when the surface is absent. Further the influence of the wind direction (particularly in yaw) on the resulting forces on the body may be

different at different ground clearance values. The objective of the present investigation was to study some of these features when the flow takes place past a three-dimensional bluff body in the presence of a ground plate.

A bluff body with a square cross-section (similar to that chosen by Nakaguchi) with a length-to-width ratio of 4 having sharp edges is utilised for the purpose. The dimensions chosen represent a simplified model of a bus body. The road surface is simulated by a surface plate and the ground clearance between the body and the surface plate is varied systematically. At each value of ground clearance the forces and moments on the body are measured and presented at several angles of yaw. Some flow visualisation experiments have also been carried out (to obtain a qualitative picture of the flow) which explain the observed features to a limited extent.

2. Experimental arrangement

All the measurements were carried out using the open jet return-circuit wind tunnel (Göttingen type) of the Fluid Mechanics Laboratory. The tunnel has a test section 1·5 m in diameter and 2·5 m long. It is provided with a six-component wire balance (semi-automatic electro-mechanical balance—Dingler make) by which all the forces and moments on the model are obtained. The model was made out of fine teak wood, 150 × 150 mm in cross-section and 600 mm long and was finished to have a smooth surface and sharp edges. It was fixed to a wooden surface plate (2·3 × 1·8 m) which in turn was held by the wires from the balance. A part of the plate (1·5 m in diameter) could be rotated to any angle required. The arrangement is schematically shown in fig.1a. The gap between the model and the surface plate was varied by fixing the model to the plate using fixtures of required heights (fig.1b). Care was taken to see that the fixtures used were flush with the model surface and offered minimum obstruction to the flow.

Experiments were carried out for the following values of the gap ratio G/H: 0, 0·05, 0·1, 0·25, 0·5 and 1. At each value of G/H forces and moments were measured over a range of yaw angle ψ varying from −10 to 40°. All the results presented correspond to the body axes system (fig.1c). The forces and moments were obtained with the model fixed to the surface plate and without the model; the difference between the two readings was used to obtain the results presented.

All the measurements were carried out at a tunnel velocity of 20 m/s which gives a Reynolds number ($U_\infty B/\vartheta$) of 2×10^5 (B is the width of the model). As the model was made with sharp edges the results in general can be expected to be independent of the Reynolds number. The velocity profile on the surface plate just in front of the model was measured (without the model in position) and the displacement thickness was found to be 5 mm. But no correction has been applied for this and there might be some influence of this on the results presented, particularly at smaller gap ratios. The turbulence level in the tunnel is 1%. No blockage correction is applied as the test section is of open type and the blockage was only about 1·5%.

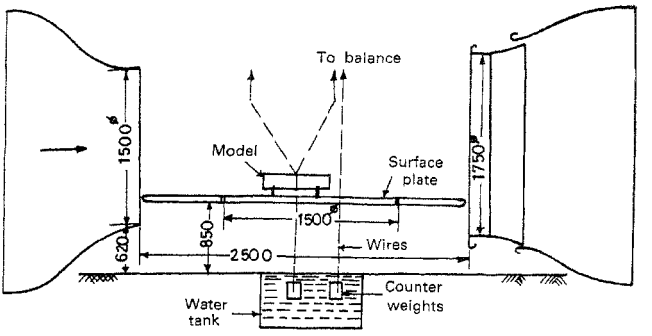

a) Wind tunnel test section.

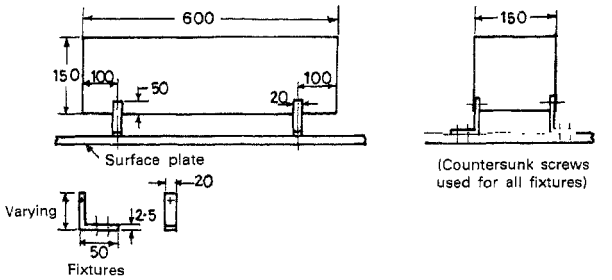

b) Model details.

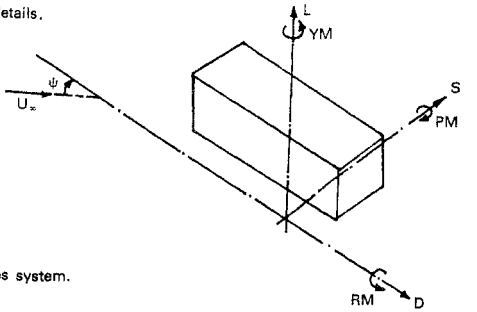

c) Body axes system.

FIG. 1. Schematic view of the experimental set-up (all dimensions are in mm).

3. Results and discussion

The variation of the six forces and moments with the gap ratio G/H at different values of the yaw angle ψ are shown in figs 2 to 7. Referring to fig. 2, it is seen that the value of C_D varies mildly with G/H at $\psi = 0$. But at other values of ψ, C_D varies considerably with G/H particularly in the region $0 < G/H < 0{\cdot}25$. Further, at lower values of ψ (10 and 20°) C_D is seen to reach a peak value around $G/H = 0{\cdot}25$ and then gradually decrease, whereas it is the reverse at $\psi = 30$ and 40° — a minimum of C_D occurs at $G/H = 0{\cdot}25$ and then it increases with G/H. The yaw angles in practice are usually less than 20° and it is significant to note that large C_D values are obtained in this range of angles at typically employed G/H ratios ($\approx 0{\cdot}2$). The result due to Muto and Ueno[3] for $G/H = 0{\cdot}4$ and $\psi = 0$ is also shown in the figure. As can be seen there is very good agreement. (The results of Muto and Ueno are for several values of L/B at $G/H = 0{\cdot}4$ and $\psi = 0$. Hence only one point is available for $L/B = 4$). The observed features could be expected to be due to changes in the wake characteristics with variation of ψ and G/H values. Some flow visualisation studies were carried out to obtain a qualitative picture of the flow which would lead to a better understanding of the observed features. These are presented and dicussed at a later stage.

The absolute magnitude of the lift coefficient C_L (fig. 3) at any angle ψ in general increases, as the body approaches the surface. This is obviously due to the increased flow velocities with narrowing gap. Also the overall magnitudes of C_L become larger at high angles of yaw showing that the fluid displacement under the body takes place at comparatively higher velocities (These points are further discussed with reference to the flow visualisation studies). It is desirable to have pressure measurements on the bottom surface of the body to obtain a clearer picture of the flow under the body.

The side force coefficient (fig. 4) is seen to increase with ψ. The extent of the separated flow region behind the body increases with the yaw angles and correspondingly the side

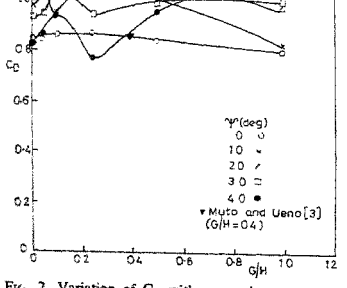

FIG. 2. Variation of C_D with gap ratio.

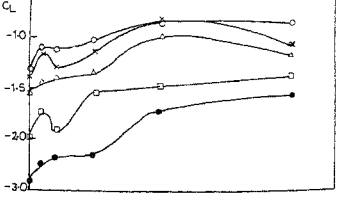

FIG. 3. Variation of C_L with gap ratio.

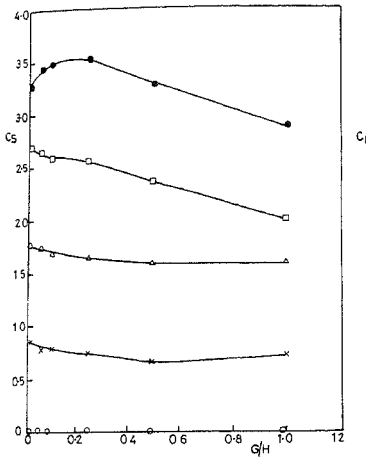

FIG. 4. Variation of C_S with gap ratio.

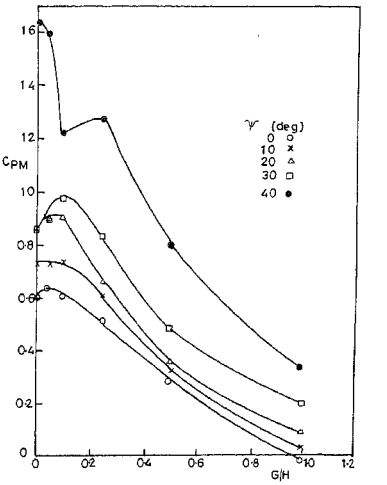

FIG. 5. Variation of C_{PM} with gap ratio.

force increases. The flow visualisation pictures (fig. 15) presented and discussed later in fact show such an increase.

The variation of the moment coefficients C_{PM}, C_{YM} and C_{RM} is shown in figs 5 to 7. At all angles of yaw the pitching moment is found to be large for $G/H \leq 0{\cdot}1$ (fig. 5) which later decreases. The overall magnitudes are higher for larger values of yaw. The

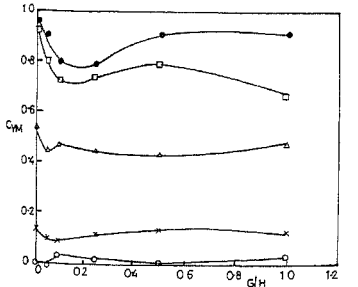

FIG. 6. Variation of C_{YM} with gap ratio.

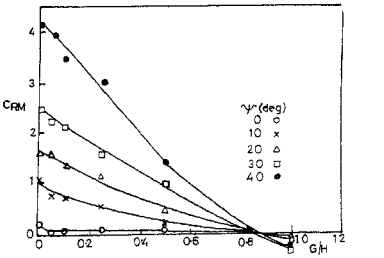

FIG. 7. Variation of C_{RM} with gap ratio.

relative increase in C_{PM} that occurs for variation in ψ from 20 to 40° is much greater than that for the change in from 0 to 20°. This could be due to the variation of the pressure field at the bottom surface across the length as the body approaches the ground plate. Further this variation can be expected to vary considerably with the yaw angle.

The yaw moment C_{YM} (fig. 6) is not very sensitive to the gap ratio G/H. But its magnitude considerably changes with ψ. Of particular interest may be the relatively large increase in yaw moment when ψ changes from 10 to 20°.

Figure 7 shows the variation of the rolling moment C_{RM}. As the gap increases the relative influence of ψ decreases and around G/H = 0·8, $C_{RM} \approx 0$. The rolling moment becomes critical when the body is quite close to the ground (G/H ≤ 0·1) even at smaller values of ψ.

The influence of the yaw angle ψ at different fixed values of G/H on the forces and moments is brought out in figs 8 to 13. When the body is at sufficiently large distance from the ground (G/H = 1, fig. 8) the value of C_D increases almost linearly with ψ. As the body approaches the surface, the drag coefficient increases initially with ψ and then

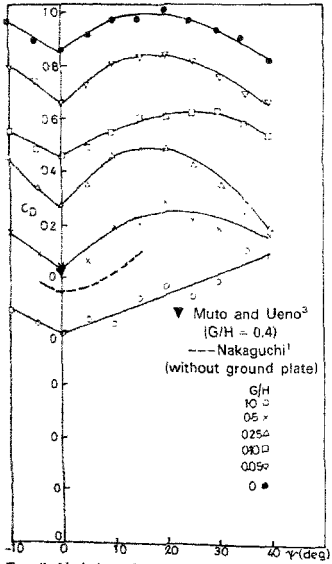

FIG. 8. Variation of C_D with yaw angle.

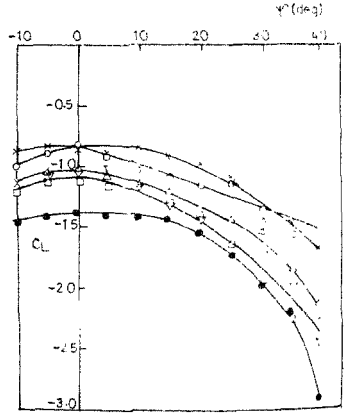

FIG. 9. Variation of C_L with yaw angle.

decreases. A peak value is seen to occur around $\psi = 20°$. The results of Nakaguchi[1] (without ground plate) and that of Muto and Ueno[3] are also shown in fig. 8. Nakaguchi's values are slightly higher than the present results for G/H = 1. As mentioned earlier, the observed variations in fig. 8 are mostly due to changes in the wake and also due to changes in the pressure distribution on the surface of the body. The magnitude of C_L increases continuously with ψ at each value of G/H (fig. 9), the increase becoming pronounced as the body approaches the ground plane particularly beyond $\psi = 20°$. As the yaw angle increases the acceleration of the flow under the body appears to increase. The side force coefficient C_S increases linearly with ψ at all G/H values. The results of Nakaguchi[1] shown in the figure also show a similar trend. The variation is seen to be nearly independent of G/H except when the body is much further away from the ground plane. The linear increase is obviously due to increase in the size of the separated region as the body is yawed more and more (revealed by the flow visualisation results).

The pitching moment (fig. 11) is seen to vary very little for value of ψ up to 20°. Beyond this angle, it increases — the rate of increase being greater when the body is closer to the ground plane. Further the magnitude of C_{PM} changes considerably for a change in G/H from 1 to 0·25. For lower values of G/H there is very little change.

This latter trend is observed in the case of rolling moment also (fig. 12). But in this

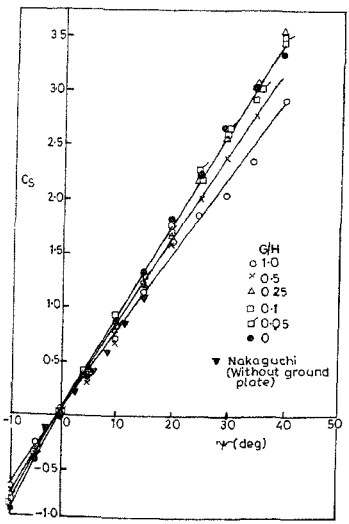

FIG. 10. Variation of C_S with yaw angle.

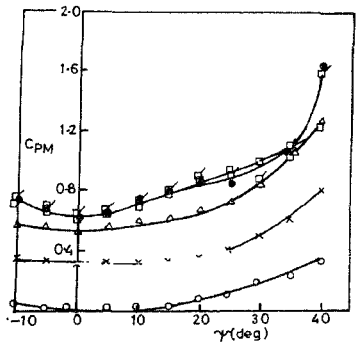

FIG. 11. Variation of C_{PM} with yaw angle.

case there is considerable variation in C_{RM} values even for $\psi < 20°$; it is nearly linear up to $\psi = 30°$ at all G/H values (except for G/H = 1), but with different slopes.

The yaw moment increases steeply with ψ at all G/H values as shown in fig. 13. But for $\psi > 30°$, the rate of increase decreases and when the body is quite close to the ground plane there is in fact a slight decrease.

The observed features in the variation of forces and moments can be attributed to basically three factors — 1) the variations in the pressure distribution on the body; 2) the changes in the structure of the wake; and 3) the displacement velocities under the body as G/H and ψ vary. The structure of the wake and under body flow are strongly dependent on each other. The accelerations under the body would be quite high as it approaches closer to the ground plane; further there could be local separation under the body which also would influence the resultant forces and moments on the body.

In order to obtain a better understanding of the observed variations in the various forces on the bluff body and also to support the three points listed earlier (to which the observed features are attributed), some flow visualisation studies were carried out in the Flow Visualisation Facility at the Fluid Mechanics Laboratory. The fluid used is water and fine aluminium powder is used as tracer particles. Experiments were conducted at a Reynolds number $\approx 10^4$. One set of experiements were carried out varying the G/H value from 0 to 1 between the body and the plate used for simulating the ground plane (fig. 14). In the second set, the flow patterns were obtained at $\psi = 0$ to 40° (fig. 15). It has to be mentioned here that the flow visualisation results presented are for two-dimensional case whereas the force field obtained is for three-dimensional case. Nevertheless the results shown in figs 14 and 15 do give a tentative explanation for the trends in the force field presented earlier as the following discussion reveals.

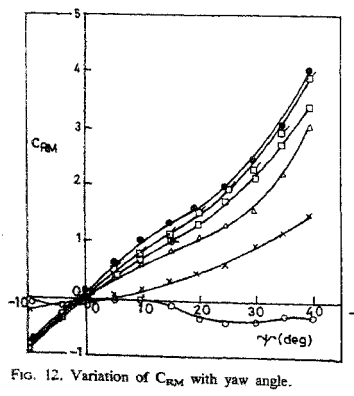

FIG. 12. Variation of C_{RM} with yaw angle.

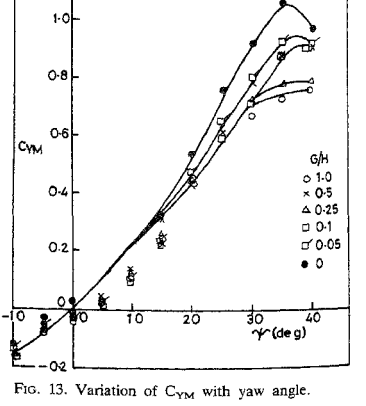

FIG. 13. Variation of C_{YM} with yaw angle.

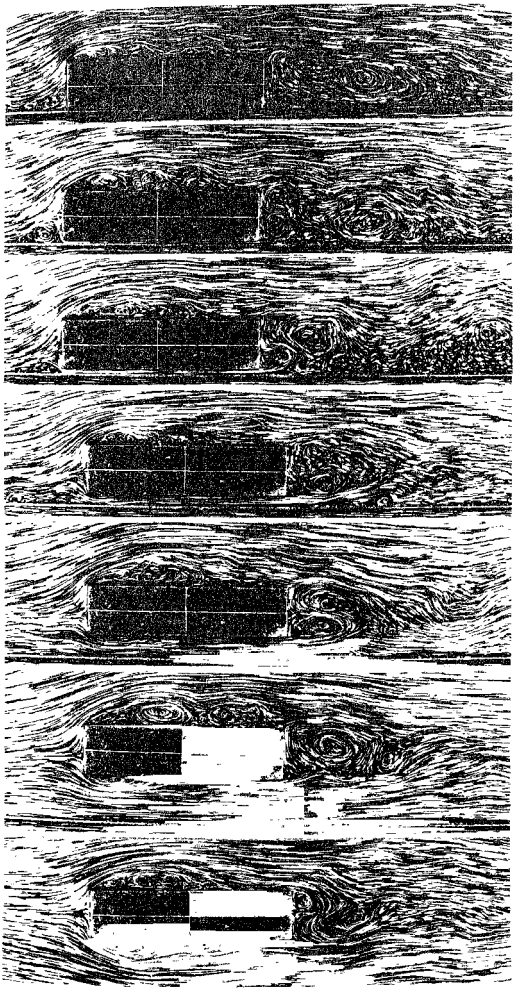

a) G/H =0

b) G/H = 0·05

c) G/H = 0·10

d) G/H = 0·25

e) G/H = 0·50

f) G/H = 1·00

g) Without ground plate ($\psi = 0°$)

FIG. 14. Typical flow patterns at different G/H ratios.

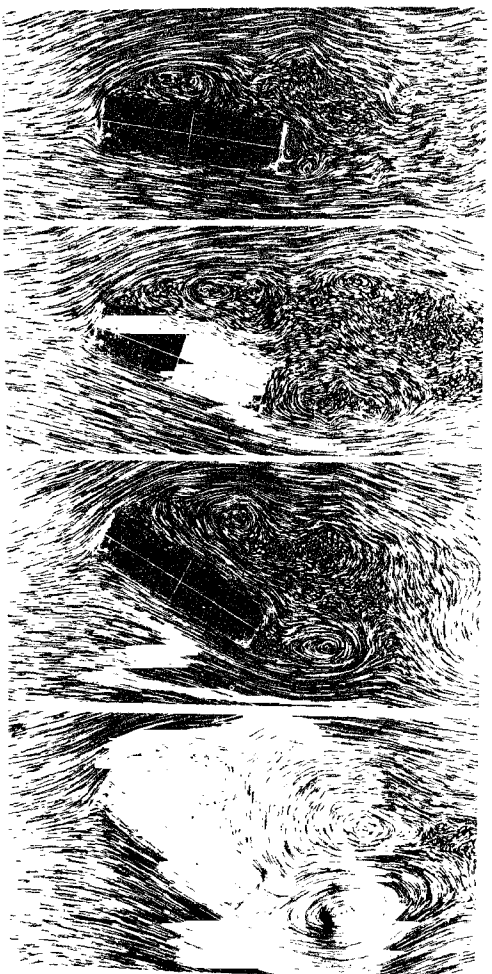

FIG. 15. Typical flow patterns at different ψ values.

Figure 14 ((a) to (f)) shows the flow patterns when the ground clearance (G/H) is varied from 0 to 1·0; fig. 14 (g) is for the case without ground plate. The position of stagnation point on the front face is seen to vary with G/H; it occurs between 0·6 and 0·7 times the height at G/H = 0 and moves down as G/H increases up to 0·10 (figs 14 a to e). It appears to move up with further increase in G/H. The separation zone that occurs in front of the body at lower gap ratios (up to G/H = 0·25) disappears at higher G/H values. A jet like flow occurs behind the body due to the ground clearance and its interaction with the wake can be clearly seen in fig. 14 (b) to (e). The size (along the flow) and the structure of the wake are considerably altered with the gap at the bottom. But the width of the wake does not alter much and the back pressure might be nearly the same in all the cases. This could be the reason for the mild variation in C_D observed with G/H at $\psi = 0$ seen in fig. 2.

At other values of ψ, the width of the wake also changes as shown in fig. 15. In fig. 8 (which shows the variation of C_D with ψ) it is seen that at most of the G/H values C_D initially increases with ψ, reaches a peak value around $\psi = 20°$ and then decreases. The correspondence between such a variation and the flow patterns shown at fig. 14(g) ($\psi = 0°$) and fig. 15(a) to (d)–ψ = 10 to 40° can be clearly seen. The wake width increases considerably up to $\psi = 20°$ beyond which it slightly reduces. Further the nature of flow at the front face is also altered. One can expect these changes to affect the pressure distribution around the body which results in the type of C_D variations shown in fig. 8. It is also interesting to see that the base flow becomes highly periodic at higher values of ψ and there is a strong current of reverse flow along the body surface at these angles (fig. 15c and d). As mentioned earlier the flow patterns shown are for two-dimensional case and in the case of a three-dimensional body there will be flow from other sides also and the flow field can be expected to be much more complex. But the two-dimensional pictures do give an idea of the changes in the wake that can be expected with variation in ψ.

The gap flows that occur between the body and the ground plate seen in fig. 14 for various values of G/H are indicative of the reasons for increase in the absolute values of C_L as the body approaces the ground plane (fig. 3). The results at fig. 14 could be taken as for $\psi = 0°$. At other values of ψ, a larger frontal area is exposed to the flow (fig. 15) and the flow on the top surface of the three-dimensional bluff body will be very much influenced by the separation that occurs at the top front edge. This and the gap flow at the underside can be expected to influence the C_L variations.

The reasons for the increase in the side force coefficient C_S with ψ seen in fig. 10 become obvious with the flow patterns shown in fig. 15. The flow pattern shown at fig. 14(g) indicates a zero side force and as ψ increases flow field is altered very much leading to an increase in C_S. It is pointed out again that there will be additional flow interactions for a three-dimensional bluff body but the pictures at fig. 15 quite clearly indicate the extent of the changes that can be expected with changes in the yaw angle.

Pressure distribution on the ground plane and on the under surface of the body would throw more light on this aspect. Wake measurements are required to clarify further the observed trends in forces and moments.

4. Concluding remarks

The results presented reveal the considerable influence of the gap ratio and the yaw angle on the aerodynamic forces and moments on a three-dimensional bluff body. The forces and moments have comparatively large magnitudes for $G/H < 0{\cdot}25$ but their variation differs; some of them (C_D, C_L, C_{YM}) show considerable variation within this gap ratio but others (C_{PM}, C_{RM}) show a steep variation beyond this gap ratio or over the entire range of gap ratios tested.

A similar trend is observed when the influence of yaw at various G/H values is considered. Some of the quantities (C_L, C_{PM}) remain nearly constant for $0 < \psi < 20°$ and increase with yaw angle beyond this. The drag coefficient increases up to $\psi = 20°$ and then decreases whereas other quantities (C_S, C_{RM}, C_{YM}) continually increase with ψ.

The flow visualisation results presented offer a tentative explanation for some of the observed features.

Though a general observation can be made that the variations seen are due to change in the pressure and flow field around the body, more experiments in these directions are required to conclusively obtain the reasons for the observed trends.

Notations

(All quantities listed refer to the body axes system as shown in fig. 1.)

C_D, C_L, C_S, C_{PM}, C_{RM}, C_{YM} : Coefficients of drag, lift, side-force, pitching moment, rolling moment, and yaw moment respectively.

G : Gap between the body and the surface plate

H : Height of the body

U_∞ : Free stream velocity

ψ : Yaw angle

References

1. Nakaguchi, H. Recent Japanese research on three-dimensional bluff body flows relevant to road-vehicle aerodynamics. In *Aerodyamic drag of bluff bodies and road vehicles*, (eds) G. Sovran, T. Morel and W.T. Mason, Plenum Press, New York, 1978.

2. Gowda, B.H.L., Gerhardt, H.J. and Kramer, C. Flow visualisation studies on three-dimensional bluff bodies. *J. Flow Visualisation Soc. Jap*, 1984, **4**(13), 56–62.

3. Mueto, S. and Ueno, H. *Report on JARI's full scale automobile wind tunnel*, JARI Technical Memo No. 56, 1976 (Not seen in original; quoted in ref. 1).